Electr Eng
DOI 10.1007/s00202-016-0441-y

ORIGINAL PAPER

Single point bearing fault diagnosis using simplified frequency model

Mohamed Lamine Masmoudi[1,2] · **Erik Etien**[1] · **Sandrine Moreau**[1] · **Anas Sakout**[2]

Received: 6 October 2015 / Accepted: 17 September 2016

Abstract The time synchronous averaging (TSA) is a well-known technique used for early detection of bearing failure in electrical machines. This method is very efficient if the characteristic default frequency is perfectly known. In this article, a reduced frequency model, derived from ESPRIT algorithm, is used to provide a very accurate estimation of the fault frequency. The precision obtained on this frequency allows to apply TSA algorithm under optimal conditions. The proposed method is tested on simulated and real vibration signals for inner and outer ring faults. Finally, a fault indicator is proposed to discriminate the healthy case from the faulty one.

Keywords Vibration · Diagnosis · Signal processing · Bearing fault · TSA · ESPRIT · Frequency estimation · Filtering

1 Introduction

Nowadays, three-phase electrical machines are widely used in industrial applications. To improve their reliability and availability, an early diagnosis has to be realized. That is why, over the last decade, several monitoring techniques have been developed and tested. The different failures which occur in electrical machines can be classified into stator, rotor or bearings faults. According to Electric Power Research Institute (EPRI), bearing faults are the most frequent faults followed by stator and rotor ones [1]. There are several reasons that can lead to bearing failure such as mechanical damages, misalignment, wear, lack or loss of lubricant and corrosion. When the smooth surfaces of rolling contact are damaged, high-stress conditions will be imposed on the surface causing a progressive deterioration of the bearing components and reducing significantly its lifetime.

Electrical machines can be supervised using several physical quantities measurements such as temperature, magnetic flux, mechanical vibrations or electrical currents [2]. Vibration analysis is clearly the preferred approach in industry to detect faulty bearings. After measurement, collected data are analyzed using signal processing methods classified into three domains: time domain analysis (with different statistics-based techniques) [3–7], frequency domain analysis (spectral analysis, cepstral analysis, envelope spectrum) [8–12] and time–frequency domain analysis (Wigner–Ville Distribution, Wavelet transform, Short-time Fourier transform and Empirical Mode Decomposition) [13–16].

The time synchronous averaging (TSA) [17–19] is well known in the field of mechanical fault detection for several decades. This approach can be interpreted as a very selective band-pass filtering around a frequency defined by the user. It allows to make a powerful cleaning of the signal to let the fault frequencies visible. However, this performance is obtained only if the fault frequency is perfectly known. In many cases, the relationships between characteristic bearing frequencies with geometric considerations cannot determine precisely the fault frequency and the results provided by TSA can induce

✉ Mohamed Lamine Masmoudi
ml_masmoudi@yahoo.com

Erik Etien
erik.etien@univ-poitiers.fr

Sandrine Moreau
sandrine.moreau@univ-poitiers.fr

Anas Sakout
anas.sakout@univ-lr.fr

1 LIAS Laboratory, University of Poitiers, B25, 2 rue Pierre Brousse, 86022 Poitiers, France

2 LaSIE Laboratory, University of La Rochelle, La Rochelle, France

Published online: 30 September 2016

the user to error. In previous works, high-resolution (HR) technics have been used to obtain this frequency with sufficient accuracy. MUltiple SIgnal Classification (MUSIC) and Estimation of Signal Parameters via Rotational Invariance Technique (ESPRIT) are the most popular methods [20–22]. To reach the desired accuracy, these methods are generally based on a frequency model with a large number of parameters. It leads to several limitations because the search over parameter space is computationally very expensive.

In this paper, a new procedure is proposed. An appropriate pre-filtering greatly reduces the model size in ESPRIT algorithm without loss of accuracy. The estimated characteristic frequency is then used to process vibration signals with TSA procedure in optimal conditions. In Sect. 2, fault characteristic frequencies expressions are defined. Time synchronous averaging method is recalled in Sect. 3. In Sect. 4, the envelope model is defined and parameters are estimated using the proposed method. Our technique is applied to experimental data in Sect. 5 and a fault indicator is presented to discriminate different faulty cases.

2 Bearing characteristic frequencies

Let us consider the case where the inner ring of a ball bearing is damaged by a failure mechanism mentioned above. Whenever one of the ball rolls on the defect, an impulsive force occurs and causes the vibration of the bearing. The bearing response (inner, outer rings) occurs at its natural frequency and it is quickly attenuated with time due to depreciation of the impulse. The fundamental frequency of vibration signal is directly linked to the ball passage on the defect.

The objective is to detect the bearing defect's fundamental frequency. It can be predicted from the bearing characteristic geometry and the rotation speed of the mechanical shaft [23].

$$\begin{cases} f_o(\text{Hz}) = f_r \dfrac{N_b}{2}\left(1 - \dfrac{D_b}{D_p}\cos\Phi\right) \\ f_i(\text{Hz}) = f_r \dfrac{N_b}{2}\left(1 + \dfrac{D_b}{D_p}\cos\Phi\right) \\ f_c(\text{Hz}) = f_r \dfrac{1}{2}\left(1 - \dfrac{D_b}{D_p}\cos\Phi\right) \\ f_b(\text{Hz}) = f_r \dfrac{D_p}{D_b}\left(1 - \dfrac{D_b^2}{D_p^2}\cos^2\Phi\right) \end{cases} \quad (1)$$

where

- f_b the characteristic frequency of a ball,
- f_i the characteristic frequency of the inner ring,
- f_o the characteristic frequency of the outer ring,
- f_c the characteristic frequency of the cage,
- f_r the rotation frequency of the mechanical shaft,
- N_b the number of balls,

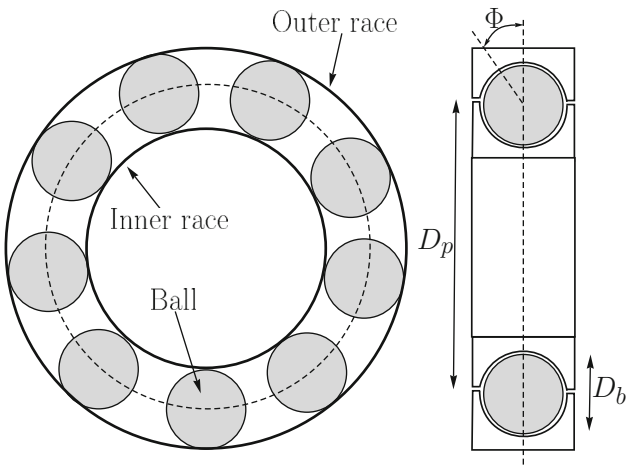

Fig. 1 Schematic diagram of a ball bearing

- D_b the ball diameter (see Fig. 1),
- D_p the pitch diameter (see Fig. 1),
- Φ the contact angle (see Fig. 1).

We consider in this work that the bearings are radial, i.e., with a contact angle $\Phi = 0°$. Moreover, these frequencies are calculated with the consideration that the contacts ball/ring are perfectly punctual and that the balls are rolling without sliding. In real bearing, the balls slide at the same time as they roll on the slopes. To take into account this sliding phenomenon, a multiplicative sliding factor of frequency is introduced, defined as the ratio between the rolling distance and the sliding distance. In practice, this factor varies between 0.96 and 0.98 for a healthy bearing and it is neglected in the present case [24].

3 Time synchronous averaging

3.1 Envelope analysis

The envelope analysis [25] is used to monitor the high-frequency response of the mechanical system with periodic shocks such as gear or bearing defects. A pulse is generated each time a component gets into contact with a defected surface of the bearing. This pulse has an extremely short duration compared to the interval between pulses. The pulse energy of the fault is distributed at a very low level over a wide range of frequencies. This wide energy distribution makes the bearing defects difficult to detect by conventional spectrum analysis, specially with the presence of external vibrations produced by other machine components. Fortunately, the impact often excites a resonance in the system at a much higher frequency than the vibrations generated by the other components. This energy distribution is generally concentrated in a narrow band

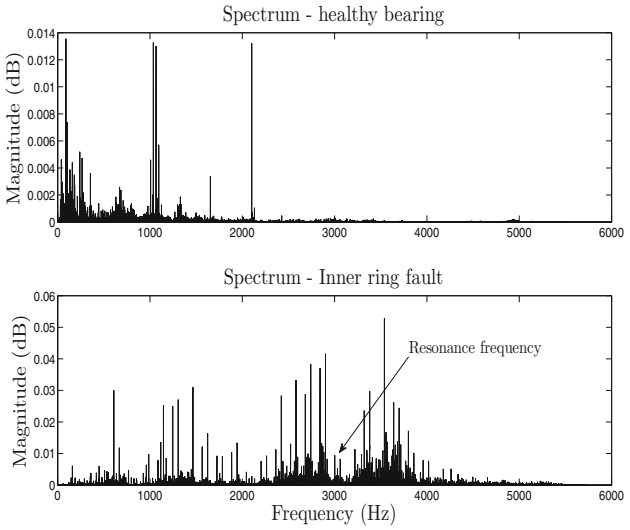

Fig. 2 The spectrum for two signals, without fault (*top*) and with an inner ring fault (*bottom*)

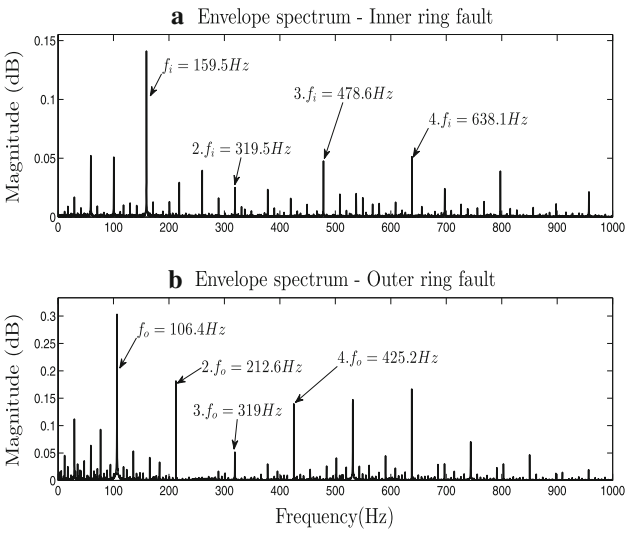

Fig. 3 The envelope spectrum for two signals with **a** inner ring fault and **b** outer ring fault

near bearing resonance which can be easily detected. Figure 2 shows two spectra calculated from vibration signals which can be found in the database of the web site "Data Bearing Center" [26]. The first spectrum (top) refers to a healthy bearing. The second signal (bottom) carries an inner ring fault. Examining this figure closely, the resonance frequency f_{res} can be identified visually around 3000 Hz.

The high-frequency technique focuses on the narrow band containing only the vibrations' fault frequencies to define the type of bearing failure. This technique consists in treating this energy with an envelope detector. First of all, data are filtered with a band-pass filter around the resonance frequency f_{res}. The center frequency of the band-pass filter should be selected to coincide with the resonance frequency of the studied spectrum. The bandwidth of the filter should be at least twice the highest characteristic frequency of the defect, this will ensure that the filter will pass the carrier frequency and at least one pair of modulation sidebands. In practice, the bandwidth should be slightly larger to accommodate the first two pairs of modulation sidebands around the carrier frequency. As a second step, the envelope of the signal is recovered by amplitude demodulation technique. The Hilbert transform is used to perform this treatment [27]. This demodulation is equivalent to translating the spectrum of the filtered signal, initially centered around the resonant frequency to 0 Hz.

The spectrum of the demodulated signal contains frequencies defined by the harmonics of the characteristic frequency f_d of the fault surrounded by multiple modulation sidebands of the shaft frequency f_r. A classical model is given in [17] to describe the spectral content of fault signals:

$$f = m.f_d + n \cdot f_r \tag{2}$$

where

- m and n are relative integers,
- f_r is the shaft frequency,
- f_d is the fault frequency (f_i for an inner ring fault or f_o for an outer ring fault).

Figure 3 shows the spectrum of the envelope signal for two distinct defects obtained from the Bearing Data Center [26]. Figure 3a illustrates the envelope signal for inner bearing fault. We can notice easily the appearance of the inner fault frequency and its harmonics (the theoretical inner fault frequency calculated using the characteristic geometry and the rotation speed corresponds to 159.93 Hz). Figure 3b represents the envelope signal for outer bearing fault. The frequency fault in this case corresponds to 106.4 Hz. Figure 4 presents a zoomed capture of the envelope signal for inner ring fault to put the emphasis on the harmonics of the inner ring characteristic frequency $n \cdot f_i = n \cdot 159.93$ Hz modulated by the shaft frequencies $f_r = 29.5$ Hz. A simple method to detect a bearing fault consists in isolating the defect frequency f_d and its harmonics. It can be performed using the Time Synchronous Averaging technique (TSA) recalled in the following section.

3.2 Time synchronous averaging (TSA)

3.2.1 Principle of TSA

It has been demonstrated in [17] that the synchronous averaging $y(t)$ of a time signal $x(t)$ using a trigger signal with the frequency f_t is equivalent to the convolution:

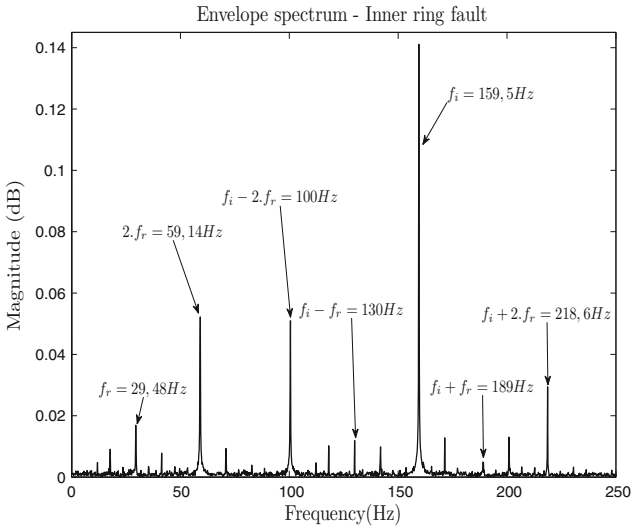

Fig. 4 Envelope spectrum of a signal with inner ring defect (zoom)

$$y(t) = x(t) * c(t) \tag{3}$$

where $c(t)$ is a train of M pulses of amplitude $1/M$, spaced with an interval of $T_t = 1/f_t$ given by [18]:

$$c(t) = \frac{1}{M} \sum_{i=0}^{M-1} \delta(t + i \cdot T_t) \tag{4}$$

In the frequency domain, $y(t)$ defined in (3) is equivalent to multiplying the Fourier transform of the signal $x(t)$ by the the Fourier transform of $c(t)$, as it is shown below:

$$Y(f) = X(f) \cdot C(f) \tag{5}$$

where $C(f)$ is the Fourier transform of $c(t)$, which can be considered as a comb filter function:

$$C(f) = \frac{1}{M} \frac{\sin(\pi M T_t f)}{\sin(\pi T_t f)} \tag{6}$$

Increasing the number of M pulses reduces the comb teeth, and reduces the amplitude of the sidelobes between teeth. For a large number of M, only exact frequency multiples of the trigger frequency f_t are passed through. Thus, the synchronous averaging can be interpreted in the frequency domain as a selective filtering that occurs at an integer multiple of the trigger frequency f_t. It also can be seen as a complete removal of all frequencies, except those which are synchronized with the frequency f_t. The selectivity of this filter increases with the number of pulses M.

Applying the TSA on the envelope signal by synchronizing the trigger with the fault frequency f_d, reduces the model (2) to:

$$f = m \cdot f_d \tag{7}$$

This filtering eliminates the multiple components of the rotational frequency f_r, combinations of the frequencies f_r and f_d and all spectral components independent of the fault. As an example, to detect the presence of an inner ring fault, the frequency of the trigger should be set to the fault frequency of the inner ring $f_t = f_i$. The TSA will select f_i and its harmonics. In the next section, a simulated signal is built to study the sensibility of TSA with trigger frequency.

3.2.2 Simulation of a reference signal

In presence of fault, the envelope signal will contain frequencies defined by the model (2). This model can be reduced to (7) only if the TSA procedure is performed with the exact default frequency. To quantify the sensibility of TSA to any error on frequency estimation, a simulation approach is proposed. A signal built with 105 frequencies (from 0 to 1267 Hz), corresponding to model (2) and defined by $0 \leq m \leq 7$ and $0 \leq n \leq 5$ is considered. The purpose of simulating a reference signal is to have a signal with the same characteristics as the real one (containing just the fault frequencies and its harmonics). So the fault frequency is well known in this case. On other hand, the simulation approach allows to add noise with a well-known signal to noise ratio (SNR) value to study the ESPRIT sensibility to noisy environment. From the Bearing Data Center, a real vibration signal corresponding to an inner ring fault ($f_d = f_i$) is used to manually estimate frequencies corresponding to the model (2). Magnitudes and phases of the inner ring fault are shown in Fig. 5. Let us note that the frequencies estimated manually are not accurate enough to be used for synchronous averaging. However, the obtained envelope signal is a good approximation of a real envelope signal and its characteristics (frequencies, magnitudes and phases) are perfectly known and can be used to study the TSA performances. Now, a reference signal (noted $x_{i\text{ref}}(t)$ in the following) is simulated by adding 105 cosines corresponding to each value (frequencies, magnitudes and phases) determined by manual procedure. Figure 6 compares the simulated signal (bottom) with the real signal (top). In the same way, a reference signal for an outer ring fault is simulated from the experimental data (noted $x_{o\text{ref}}(t)$).

3.2.3 Application of TSA

Table 1 shows the difference between the theoretical $f_{i.\text{theo}}$ and the real fault frequency $f_{i.\text{real}}$ of the inner ring. The theoretical frequencies are calculated using the bearing characteristic geometry and the rotation speed of the mechanical shaft. The real fault frequencies are determined by manual procedure. It can be seen in this table that the error increases with the harmonics. In this work, the number of pulses $M = 50$ is chosen so that the pulse width is greater

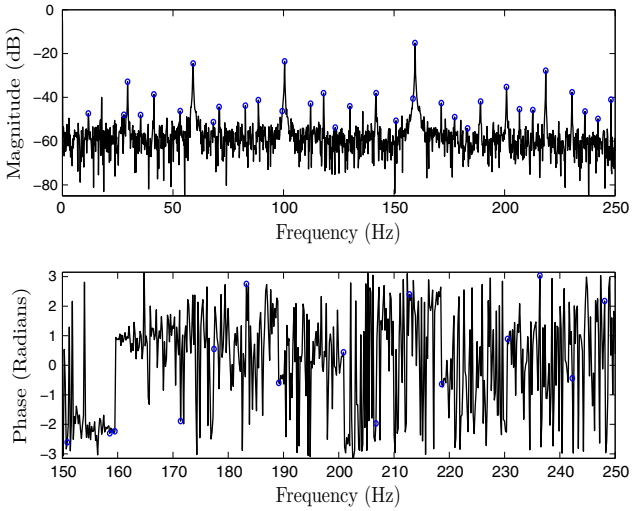

Fig. 5 Zoom of envelope spectrum of a signal with inner ring fault. Markers *o* show frequencies, magnitudes and phases estimated by manual procedure

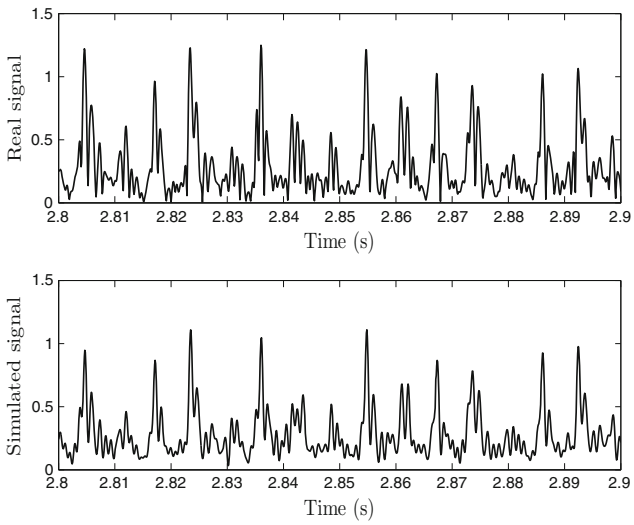

Fig. 6 Vibration signals spectrum with inner ring fault, real signal (*top*) and simulated signal (*bottom*)

than the double of the expected maximum deviation (in our case it has been chosen greater than $2 \times 2\,\text{Hz} = 4\,\text{Hz}$).

In the following, TSA is applied to the two simulated reference signals $x_{i\text{ref}}(t)$ and $x_{o\text{ref}}(t)$. The used trigger frequency f_t is the true inner ring characteristic frequency. The results are shown in Fig. 7 where the inner ring fault can be clearly identified. The characteristic frequency f_i and its harmonics have been well isolated by TSA filtering. As expected, in the case of an outer ring fault, the chosen trigger $f_t = f_i$ is not adapted for this case and the characteristic frequencies are eliminated by the TSA procedure, except the frequencies corresponding coincidentally to the inner ring frequency and its harmonics ($3f_o = 2f_i \cong 318\,\text{Hz}$, $6f_o = 4f_i \cong 636\,\text{Hz}$, $9f_o = 6f_i \cong 954\,\text{Hz}$). At this stage, it is improbable to

Table 1 Deviation between theoretical and estimated frequencies of a signal with inner ring defect

	f_i	$2f_i$	$3f_i$	$4f_i$	$5f_i$
$f_{i.\text{theo}}$ (Hz)	159.9	319.86	479.79	639.7	799.6
$f_{i.\text{real}}$ (Hz)	159.55	319.15	478.64	638.12	797.6
$\lvert\delta f\rvert$	0.35	0.71	1.15	1.58	2
Err (%)	0.21	0.22	0.24	0.24	0.25

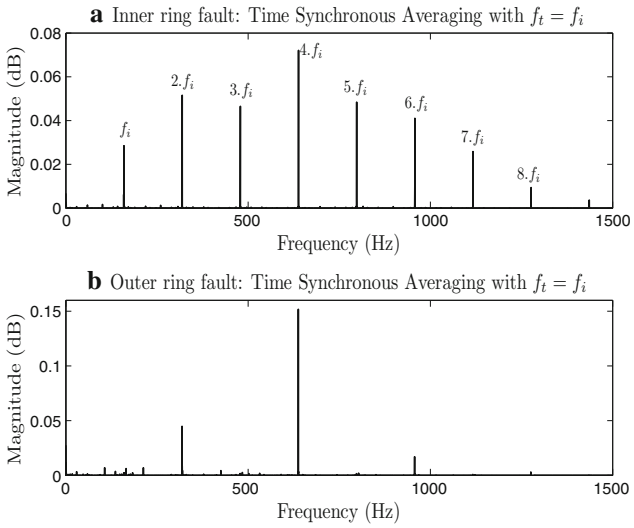

Fig. 7 The average spectrum for the reference signals $x_{i\text{ref}}(t)$, $x_{o\text{ref}}(t)$ with $f_t = f_i$. **a** For inner ring fault and **b** for outer ring fault

conclude that the inner ring is damaged. This exceptional equality can be explained by the fact that the ratio between *the pitch Diameter* and the *ball Diameter* is equal to 5 (according to the geometric characteristics of the bearing 6205-2RS JEM SKF: $N_b = 9$, $D_{\text{ball}} = 7.94\,\text{mm}$, $D_{\text{pitch}} = 39\,\text{mm}$, $\Phi = 0°$). The Eq. (1) defined in Sect. 2 becomes:

$$\begin{cases} f_o(\text{Hz}) = f_r \dfrac{N_b}{2}\left(\dfrac{4}{5}\right) \\ f_i(\text{Hz}) = f_r \dfrac{N_b}{2}\left(\dfrac{6}{5}\right) \end{cases} \tag{8}$$

According to this equation, the frequencies $3f_o, 6f_o, 9f_o$ are respectively equal to $2f_i$, $4f_i$, $6f_i$ for $\frac{D_p}{D_b} = 5$. In the Sect. 5.1, a procedure has been established to discriminate inner bearing fault from other cases.

Now, let us consider the case where the theoretical characteristic frequency is not determined precisely. Indeed, several parameters in (1) can be poorly calculated or measured such as the rotation frequency (f_r). In these cases, the trigger frequency is different from the real characteristic. Figure 8 shows the results obtained with $f_t = 0,97 f_i$ (error of 3 %). It can be seen that a correct fault identification cannot be obtained. The use of time synchronous averaging with the-

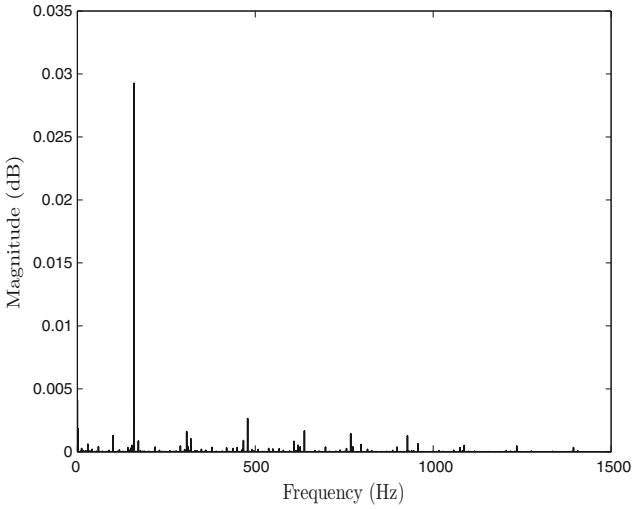

Fig. 8 The spectrum of the reference signals $x_{i\text{ref}}(t)$ with $f_t = 0,97 \cdot f_i$ for inner ring fault

oretical characteristic frequency does not guarantee that the result is exploitable. The fault frequency must be estimated with a high precision to extract the faulty cases from healthy ones. In the following, a high-resolution method is performed to determine precisely this frequency.

4 Identification of the characteristic frequency using a high-resolution method

4.1 ESPRIT method: general framework

The acronym **ESPRIT** stands for **E**stimation of **S**ignal **P**arameters via **R**otational **I**nvariance **T**echnique. ESPRIT is an approach based on subspace techniques which are known to be very powerful estimation techniques [28]. The purpose of using ESPRIT is to estimate the parameters of the signal modeled in (9) and particularly, to estimate the frequency modulations induced by the bearing fault. This technique is based on a decomposition of the signal $x(t)$ into two eigenspaces: the signal generated by the damped sinusoidal components $s(t)$ and noise subspace $x_k(t)$ forming its orthogonal complementary subspace.

$$\begin{aligned} x(t) &= s(t) + x_k(t) \\ &= \sum_{k=0}^{K-1} a_k e^{-\delta_k t} e^{i(\omega_k t + \varphi_k)} + x_k(t) \\ &= \sum_{k=0}^{K-1} \alpha_k z_k^t + x_k(t) \end{aligned} \tag{9}$$

The complex parameters $\alpha_k = a_k e^{i\varphi_k}$, $z_k = e^{-\delta_k} e^{i\omega_k}$ are, respectively, the amplitude and the pole of the kth component of the signal $s(t)$. The parameter a_k represents the amplitude at the origin, φ_k the phase at the origin, δ_k the damping and ω_k the pulsation. In general case, these four parameters have to be estimated for the K components of the signal. In this work, the pulsation $\omega_k = 2\pi f_k$ implies that the frequency $f_k = \omega_k/2\pi$ has to be determined with high precision.

As a first step, the Hankel matrix is calculated from the discrete signal (9) [28,29].

$$X(t) = \begin{bmatrix} x_{t-l+1} & x_{t-l+2} & \cdots & x_t \\ x_{t-l+2} & & & x_{t+1} \\ \vdots & & & \vdots \\ x_{t-l+n} & x_{t-l+n+1} & \cdots & x_{t+n-1} \end{bmatrix} \tag{10}$$

where the integers l and n are defined as $N = n + l - 1$ samples of the signal (in the application of this algorithm $n = l = N_t$). Applying the singular value decomposition (SVD) on the Hankel matrix, a diagonal matrix S of the same dimension as X, and unitary matrices U and V are calculated so that $X = U \cdot S \cdot V^T$.

ESPRIT algorithm is based on a strong property, rotational invariance of space signal. Define the two matrices $U_\uparrow$, $U_\downarrow$ of dimension $K - 1$ containing, respectively, the $K - 1$ last rows and the $K - 1$ first rows of the matrix U, where K is the length of the eigenvalues vector $\{z_k\}$ of the model.

After determining the two matrices $U_\uparrow, U_\downarrow$, the calculation of the spectral matrix is given by (11), where $(^\dagger)$ is referred to the pseudoinverse of the matrix.

$$\phi(t) = (U_\downarrow)^\dagger \cdot U_\uparrow \tag{11}$$

In particular, the eigenvalues of the spectral matrix $\phi(t)$ are the eigenvalues $\{z_k\}_{k=0,1,\ldots,K-1}$ of the model. Once the complex poles are determined, the damping δ_k and the frequency f_k can be calculated by:

$$\delta_k = -\ln(|z_k|) \tag{12}$$

$$f_k = \frac{1}{2\pi} \arg(z_k) \tag{13}$$

As a second step, the Vandermonde matrix V^n of dimension $K \times n$ is calculated using the complex poles determined before as follows:

$$V^n = \begin{bmatrix} 1 & 1 & \cdots & 1 \\ z_1 & z_2 & \cdots & z_K \\ \vdots & & & \vdots \\ z_1^{n-1} & z_2^{n-1} & \cdots & z_K^{n-1} \end{bmatrix} \tag{14}$$

where

- K is the length of the eigenvalues vector $\{z_k\}$ of the model.

The complex amplitude α_k is calculated by multiplying the pseudoinverse of the matrix V^n by the $x(t)$ as it is shown in (15). This leads to the determination of the amplitude a_k and the phase φ_k at the origin.

$$\alpha_k = (V^n)^{\dagger} \cdot x(t) \tag{15}$$

$$a_k = |\alpha_k| \tag{16}$$

$$\varphi_k = \arg(\alpha_k) \tag{17}$$

This method will be applied to the envelope of the vibration signals to determine all the parameters of the model (9) and especially to estimate the fault frequencies. This method will be implemented in MATLAB environment and applied to different vibrations signals to identify the defects of the outer or the inner rings.

4.2 Algorithm simplification by pre-filtering

High-resolution methods are very efficient for signals containing a large number of spectral components. The richer in frequency components the signal is, the higher the number of model frequencies characterizing the signal. It leads to large matrices (the Hankel matrix $N_t \times N_t$ will have a large dimension) and long computation times. In our case, only the fault characteristic frequency is needed with high precision. Consequently, ESPRIT algorithm can be simplified and the number of model frequencies considerably reduced (reducing the length of the eigenvalues vector K). However, the signal must be pre-filtered to limit the range of the analysis around the characteristic frequency.

To find optimal values for parameters N_t (order of the Hankel matrix) and K (length of the eigenvalues vector $\{z_k\}$), a white noise $x_k(t)$ is added to the reference signal:

$$x_{\text{ref}k}(t) = x_{\text{ref}}(t) + x_k(t), \tag{18}$$

where $x_{\text{ref}}(t)$ represents the signal built in Sect. 3.2.2. The magnitude of $x_k(t)$ is tuned to obtain a desired signal to noise ratio defined by:

$$\text{SNR(dB)} = 10\log\left[\frac{\text{RMS}(x_{\text{ref}})}{\text{RMS}(x_k)}\right]^2, \tag{19}$$

with RMS(x) defined as the root mean square of the signal $x(t)$.

$x_{\text{ref}k}(t)$ is now filtered around the desired characteristic frequency (f_i). Results are shown in Table 2, respectively, for $K = 3$ and 2 and $N_t = 30$ and 3. Estimations of the characteristic frequency are performed on the one hand for the reference signal (inner ring fault) without band-pass filtering. On the other hand, this estimation is made with a pre-filtered signal. The relative error is given as:

Table 2 Characteristic frequency estimation: optimal parameters for an inner ring defect ($f_d = f_i$)

		SNR (dB)			
		-1	0	1	10
Witouth filtering	K	3	3	3	3
	N_t	30	30	30	30
	$Err(\%)$	0,98	0,93	0,86	0,8
	Calculation time $= 1,74s$				
With pre-filtering	K	2	2	2	2
	N_t	3	3	3	3
	$Err(10^{-3}\%)$	8	4,6	0,85	0,5
	Calculation time $= 0,6s$				

$$\text{Err} = \frac{f_{\text{real}} - f_{\text{est}}}{f_{\text{real}}} \times 100 \tag{20}$$

where

- f_{real} is the real frequency.
- f_{est} is the estimated one.

It can be seen that the pre-filtering around f_i plays an important role in the precision of the estimated frequency: it reduces the frequency components around f_i and makes its identification easier by choosing the highest amplitude of those components. It reduces also the matrix dimensions calculated in the ESPRIT algorithm and consequently reduces the computation time. It can be seen also in Table 2 the impact of the noise on the proposed technique where the error is decreasing (decreasing from 8×10^{-3} to 5×10^{-4} %) with the increase of the SNR. On the simulated signal, the characteristic frequency is obtained with a very good accuracy for $K = 2$ and $N_t = 3$ (an error about 10^{-4} %), which indicates the poor influence of the noise on the proposed technique.

4.3 Influence of the contact angle Φ

The proposed technique is applied on inner ring fault signals by introducing an error on the contact angle Φ to prove its effectiveness regardless of the error introduced during the measurement.

It can be noted in Table 3 that the calculated characteristic frequency f_{ith} varies for each contact angle value unlike

Table 3 Influence of contact angle Φ on the estimation of characteristic frequency

	The calculated f_{ith} (Hz)	The estimated $\hat{f}_i$ (Hz)
$\Phi = 0°$	159.92	159.54
$\Phi = 10°$	159.52	159.54
$\Phi = 20°$	158.30	159.54

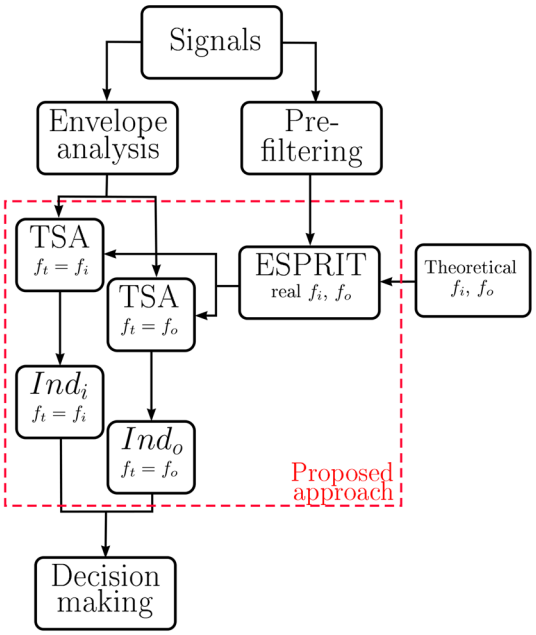

Fig. 9 The proposed approach for single bearing fault detection

the estimated frequency $\hat{f}_i$. This means that the proposed technique is totally independent of the contact angle value. In the next section, this methodology will be used for fault detection on real data.

5 Experimental results

The MATLAB environment is used to implement the proposed technique. According to previous sections, the following procedure is proposed to detect single point bearing failure using vibration signals (Fig. 9):

1. Band-pass filtering of the signal around the resonance frequency f_{res};
2. Calculation of the Hilbert transform and the envelope signal;
3. Band-pass filtering of the envelope signal around the theoretical characteristic frequency f_d;
4. Characteristic frequency estimation using pre-filtering and simplified ESPRIT algorithm;
5. Time synchronous averaging of the envelope signal with the estimated characteristic frequency;
6. Decision making by calculating a fault indicator.

Table 4 shows results for experimental data from the Bearing Data Center [26]. Two bearings with inner ring fault are tested. The diameter of the artificial pit made on the inner ring varies from 0.007 to 0.021 in. In the following, this diameter is called "fault diameter". According to Sect. 4.2, the following parameters are chosen for the ESPRIT algorithm $K = 2$ and $N_t = 3$ as optimal values to achieve enough accuracy as well as suitable computation time. The rotation frequency of the mechanical shaft is $f_r = 29.53$ Hz. According to (1), the theoretical characteristic frequency of the inner ring is $f_{ith} = 159.93$ Hz.

Table 4 Inner ring fault: characteristic frequency estimation using pre-filtering and ESPRIT algorithm

	$f_{ith} = 159.93$ Hz	
Fault diameter (in.)	0.007	0.021
Estimated frequency (Hz)	159.54	159.79

Table 5 Outer ring fault: characteristic frequency estimation using pre-filtering and ESPRIT algorithm

	$f_{oth} = 105.87$ Hz	
Fault diameter (in.)	0.007	0.021
Estimated frequency (Hz)	106.29	106.03

The same tests are realized for an outer ring fault. The results are given in Table 5. In this case, the theoretical characteristic frequency of the outer ring is $f_{oth} = 105.87$ Hz.

5.1 Results of TSA application

Tables 4 and 5 show that the simplified ESPRIT algorithm gives a good estimation of the characteristic frequencies. These frequencies can now be used to perform the TSA filtering with the required accuracy. Figures 10 and 11 show the results of TSA applied to faulty bearings with frequencies shown in Tables 4 and 5. Characteristic frequencies and their harmonics are correctly isolated and all external components are filtered which leads to a clean signal containing just information about the bearing fault.

The proposed technique has also proved its effectiveness in function of different operating points when the motor load was increased from 0 to 3 hp and the rotation speed was slightly reduced from 1797 to 1730 rpm. Figure 12 shows the results of applying TSA technique on inner bearing fault signals with different motor load. According to this figure, the characteristic frequency and its multiples are perfectly isolated.

Finally, a bearing fault indicator is proposed to distinguish the faulty case from the healthy one by calculating the sum of the maximum amplitude of the signal $Y(f)$ defined in (5) for $f = n \cdot f_d$ as it is shown in (21). This indicator is applied to signals with inner ring fault, outer ring fault and healthy signals for different motor loads.

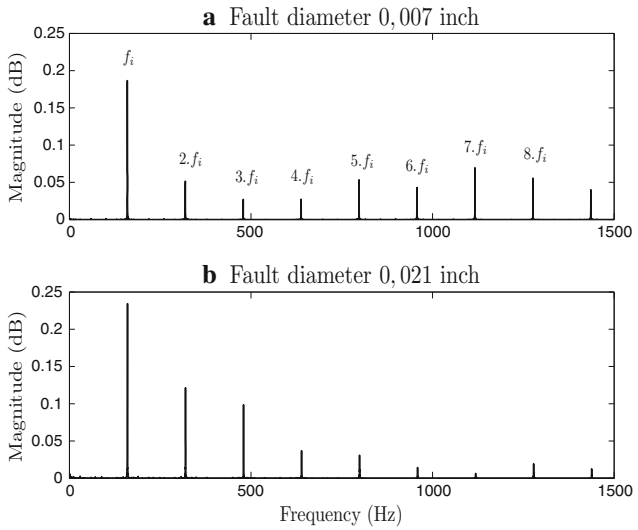

Fig. 10 The average spectrum for an inner ring fault with two different fault diameters **a** 0.007 and **b** 0.021 in. ($M = 50$)

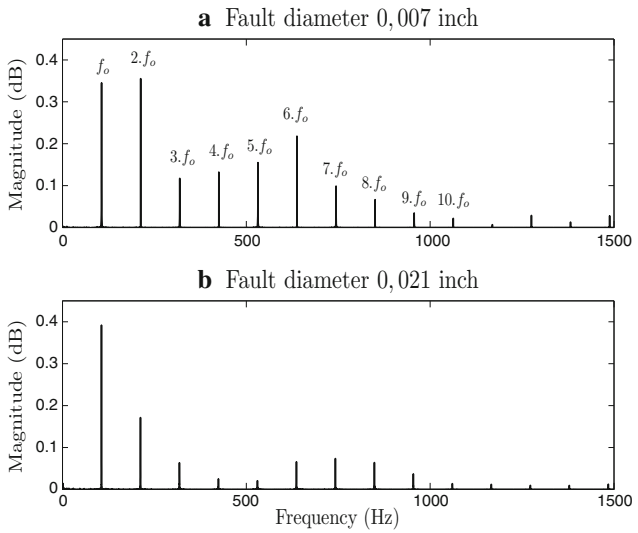

Fig. 11 The average spectrum for an outer ring fault with two different fault diameters **a** 0.007 and **b** 0.021 in. ($M = 50$)

$$\text{Ind} = \sum_{n=1}^{10} Y(n \cdot f_d) \tag{21}$$

where

- f_d represents one of the characteristic frequencies (f_i or f_o).
- n represents the multiples of the characteristic frequency.

Figure 13 shows the evolution of the proposed indicator for several cases with $f_d = f_i$. A threshold ($\text{ind}_{\text{th}} = 0.2$) is chosen as twice the maximum amplitude of the indicator value when applying the TSA on the outer ring fault signal.

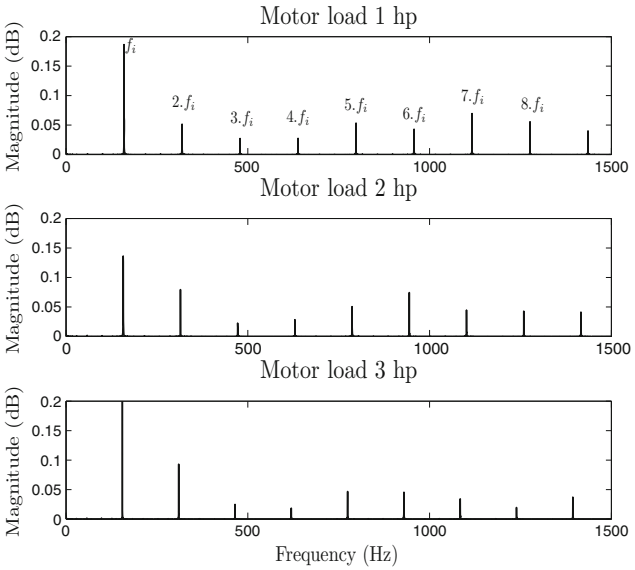

Fig. 12 The average spectrum for inner bearing fault with **a** 1 hp motor load, **b** 2 hp motor load and **c** 3 hp motor load

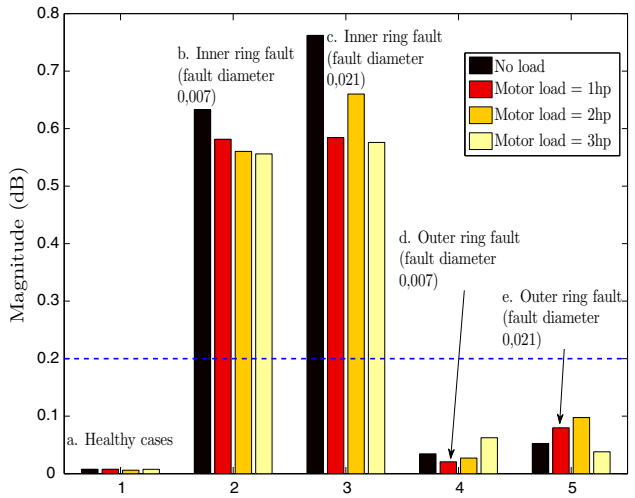

Fig. 13 Evolution of the indicator Ind for *a* healthy signal, *b* signal with 0.007 in. inner ring fault diameter, *c* signal with 0.021 in. inner ring fault diameter, *d* signal with 0.007 in. outer ring fault diameter and *e* signal with 0.021 in. outer ring fault diameter

This figure proves that the proposed indicator can clearly distinguish the inner ring fault from others cases.

Figure 14 shows the evolution of the proposed indicator for several cases with $f_d = f_o$. This figure illustrates the effectiveness of the proposed indicator which can clearly discriminate the outer ring fault from others cases.

Figure 9 resumes the proposed technique. It allows detecting single bearing fault. To characterize the fault (defected component, fault severity) two steps are required. The first one is the estimation of the real fault frequency which is mostly different from the theoretical one using ESPRIT algorithm. The second step is vibration signals filtering from all

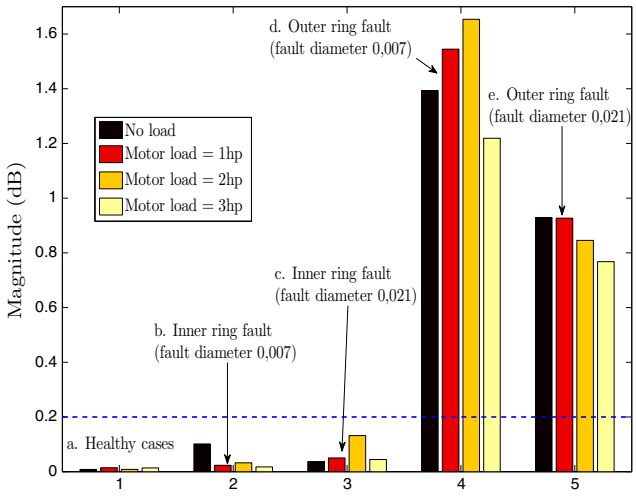

Fig. 14 Evolution of the indicator Ind for *a* healthy signal, *b* signal with 0.007 in. inner ring fault diameter, *c* signal with 0.021 in. inner ring fault diameter, *d* signal with 0.007 in. outer ring fault diameter and *e* signal with 0.021 in. outer ring fault diameter

spectral components except those which coincide with real fault frequencies and their harmonics (respectively, f_i and f_o). Once the TSA is applied, an indicator Ind is calculated for the two fault frequencies. The final step of this procedure is decision making by evaluating the calculated indicator. If the indicator exceeded a certain threshold, the bearing will be considered defected, otherwise it is healthy.

6 Conclusion

This paper deals with the improvement of time synchronous averaging using a simplified ESPRIT algorithm applied to simulated and real vibration signals. The simplification has been obtained by a pre-filtering of the envelope signal around the fault frequency. ESPRIT algorithm has been also considerably simplified and the number of model frequencies reduced to the minimum by choosing optimal values for the two parameters N_t and K to achieve enough accuracy as well as fast calculation time. Finally, the resulting algorithm is very fast and provides very accurate fault frequencies. This accuracy permits to use these frequencies in a TSA filtering with good performances. This algorithm is applied to vibration signals with inner and outer ring faults and different fault diameters. The obtained results confirm that the combination between TSA, ESPRIT and the pre-filtering achieves better performances than the only application of TSA to vibration signals. The proposed algorithm shows its efficiency for detection of the inner and the outer ring fault for different fault diameters. The proposed procedure is able to distinguish inner from outer faults by setting the trigger frequency f_t equal to the fault characteristic frequencies. If the obtained frequencies are not a train of this characteristic frequency and its harmonics, then the bearing is considered healthy. The proposed indicator is characterized by its simplicity and effectiveness. The results show its capability of distinguishing the inner ring bearing fault from the outer ring bearing fault and the healthy bearing for different fault diameters and motor loads.

The proposed approach was successfully tested for single point bearing faults with various fault cases and load conditions. Further investigations are required to study the generalized roughness faults (multi-point bearing faults).

Acknowledgments This work has been realized through the collaboration between LaSIE laboratory, University of La Rochelle, France and LIAS laboratory, University of Poitiers, France, with the financial support of FEDER program no: 33288-2010.

References

1. Report of large motor reliability survey of industrial and commercial installations, part I. IEEE Trans Ind Appl IA-21(4):853–864 (1985)
2. Jin X, Zhao M, Chow TWS, Pecht M (2014) Motor bearing fault diagnosis using trace ratio linear discriminant analysis. IEEE Trans Ind Electron 61(5):2441–2451
3. Prieto MD, Cirrincione G, Espinosa AG, Ortega JA, Henao H (2013) Bearing fault detection by a novel condition-monitoring scheme based on statistical-time features and neural networks. IEEE Trans Ind Electron 60(8):3398–3407
4. Harmouche J, Delpha C, Diallo D (2014) Incipient fault detection and diagnosis based on Kullback–Leibler divergence using principal component analysis: part I. Signal Process 94:278–287
5. Picot A, Obeid Z, Régnier J, Poignant S, Darnis O, Maussion P (2014) Statistic-based spectral indicator for bearing fault detection in permanent-magnet synchronous machines using the stator current. Mech Syst Signal Process 46(2):424–441
6. Harmouche J, Delpha C, Diallo D (2015) Incipient fault detection and diagnosis based on Kullback–Leibler divergence using principal component analysis: part II. Signal Process 109:334–344
7. Li M, Yang J, Wang X (2015) Fault feature extraction of rolling bearing based on an improved cyclical spectrum density method. Chin J Mech Eng 28(6):1–8
8. Kunli M, Yunxin W (2011) Fault diagnosis of rolling element bearing based on vibration frequency analysis. Third international conference on measuring technology and mechatronics automation (ICMTMA), vol 2, pp 198–201
9. Zhang X, Kang J, Bechhoefer E, Teng H (2014) Enhanced bearing fault detection and degradation analysis based on narrowband interference cancellation. Int J Syst Assur Eng Manag 5(4):645–650
10. Hecke B, Qu Y, He D, Bechhoefer E (2014) A new spectral average-based bearing fault diagnostic approach. J Fail Anal Prev 14(3):354–362
11. El Bouchikhi EH, Choqueuse V, Benbouzid MEH (2015) Induction machine faults detection using stator current parametric spectral estimation. Mech Syst Signal Process 52:447–464
12. Labar H, Zerzouri N, Kelaiaia M (2015) Wind turbine gearbox fault diagnosis based on symmetrical components and frequency domain. Electr Eng 97(4):327–336

13. Bendjama H, Bouhouche S, Boucherit MS (2012) Application of wavelet transform for fault diagnosis in rotating machinery. Int J Mach Learn Comput 2(1):82–87
14. Yan R, Gao RX, Chen X (2014) Wavelets for fault diagnosis of rotary machines: a review with applications. Signal Process 96:1–15
15. Georgoulas G, Loutas T, Stylios CD, Kostopoulos V (2013) Bearing fault detection based on hybrid ensemble detector and empirical mode decomposition. Mech Syst Signal Process 41(1):510–525
16. Muhammad I, Nordin S, Rosdiazli I, Vijanth SA, Hung NT, Magzoub MA (2015) Analysis of bearing surface roughness defects in induction motors. J Fail Anal Prev 15(5):730–736
17. McFadden PD, Toozhy MM (2000) Application of synchronous averaging to vibration monitoring of rolling element bearings. Mech Syst Signal Process 14(6):891–906
18. McFadden PD (1984) Model for the vibration produced by a single point defect in a rolling element bearing. J Sound Vib 96(1):69–82
19. Zhan Y, Makis V (2006) A robust diagnostic model for gearboxes subject to vibration monitoring. J Sound Vib 290(3):928–955
20. Akbar MA, Tila HB, Khalid MZ, Ajaz MA (2009) Bit error rate improvement using ESPRIT based beamforming and RAKE receiver. IEEE 13th international multitopic conference (INMIC), pp 1–6
21. Dhope TS, Simunic D (2013) On the performance of DoA estimation algorithms in cognitive radio networks: a new approach in spectrum sensing. 36th International convention on information & communication technology electronics & microelectronics (MIPRO), pp 507–512
22. Gökta T, Arkan M, Özgüven ÖF (2015) Detection of rotor fault in three-phase induction motor in case of low-frequency load oscillation. Electr Eng 97(4):337–345
23. Schoen RR, Habetler TG, Kamran F, Bartfield RG (1995) Motor bearing damage detection using stator current monitoring. Trans Ind Appl 31(6):1274–1279
24. Lindh T, Ahola J, Kamarainen JK, Kyrki V, Partanen J (2003) Bearing damage detection based on statistical discrimination of stator current. IEEE symposium on diagnostics for electric machines, power electronics and drives, pp 177–181
25. Immovilli F, Bellini A, Rubini R, Tassoni C (2010) Diagnosis of bearing faults in induction machines by vibration or current signals: a critical comparison. IEEE Trans Ind Appl 46(4):1350–1359
26. Case Western Reserve University Bearing Data Center Website. http://csegroups.case.edu/bearingdatacenter/home
27. Marple SL (2003) Computing the discrete-time analytic signal via FFT. IEEE Trans Signal Process 47(9):177–181
28. Roy RH, Kailath T (1989) ESPRIT—estimation of signal parameters via rotational invariance techniques. IEEE Trans Acoust Speech Signal Process 37(7):984–995
29. Badeau R, Bertrand D, Richard G (2006) A new perturbation analysis for signal enumeration in rotational invariance techniques. IEEE Trans Signal Process 54(2):450–458